A 5G/GNSS Integrated Positioning Method

Chengming Jin, Wee Peng Tay, Kai Zhao, Keck Voon Ling and Kok Kee Sin
Nanyang Technological University (NTU), Singapore

BIOGRAPHY

Chengming Jin received the B.Eng. degree in Automation and Ph.D. degree in Traffic Information Engineering & Control from Beijing Jiaotong University, China, in 2010 and 2019 respectively. His research interests include multi-sensor fusion, Global Navigation Satellite System (GNSS), train control system and safety, 5G communications and localization. From 2015 to 2017, he was a visiting Ph.D. candidate in the University of Melbourne, Australia. Since 2019, he is a Research Fellow at the School of Electrical and Electronic Engineering, Nanyang Technological University, Singapore.

Wee Peng Tay received the B.S. degree in Electrical Engineering and Mathematics, and the M.S. degree in Electrical Engineering from Stanford University, Stanford, CA, USA, in 2002. He received the Ph.D. degree in Electrical Engineering and Computer Science from the Massachusetts Institute of Technology, Cambridge, MA, USA, in 2008. His research interests include information and signal processing over networks, distributed inference and estimation, information privacy, machine learning, information theory, and applied probability. He is currently an Associate Professor at the School of Electrical and Electronic Engineering, Nanyang Technological University, Singapore. Dr. Tay received the Tan Chin Tuan Exchange Fellowship in 2015. He is a coauthor of the best student paper award at the Asilomar conference on Signals, Systems, and Computers in 2012, and the IEEE Signal Processing Society Young Author Best Paper Award in 2016. He was an Associate Editor for the IEEE Transactions on Signal Processing (2015 – 2019), and is currently an Associate Editor for the IEEE Transactions on Signal and Information Processing over Networks, an Editor for the IEEE Transactions on Wireless Communications and IEEE Open Journal of Vehicular Technology. He serves on the Machine Learning for Signal Processing Technical Committee of the IEEE Signal Processing Society.

Kai Zhao received the B.Eng. degree in Electrical Engineering and Automation from Huazhong University of Science and Technology, China in 2017, and M.Sc. degree in Electrical Engineering from National University of Singapore in 2019. His research interests include statistical signal processing and machine learning. He is currently a Research Associate at the School of Electrical and Electronic Engineering, Nanyang Technological University, Singapore.

Keck Voon Ling received the Ph.D. degree from the University of Oxford in 1992. His research interests include model predictive control and moving horizon estimation, their embedded implementation, and applications to fast dynamic systems. In recent years, he has been applying his research to multi-band GNSS software receivers, as well as navigation and positioning applications. He is currently an Associate Professor at the School of Electrical and Electronic Engineering, Nanyang Technological University, Singapore.

Kok Kee Sin was a Senior Research Engineer from the SMRT-NTU lab. He was responsible for the design and development of a sensor systems for SMRT door actuator. He is presently a Research Associate with the COSMO lab doing design and development of GNSS multi-frequency system for auto-navigation vehicle at the School of Electrical and Electronic Engineering, Nanyang Technological University, Singapore.

ABSTRACT

The emergence of the fifth generation (5G) positioning provides a promising opportunity to augment global navigation satellite system (GNSS) in some GNSS-challenged environments. This paper presents a 5G code and carrier phase receiver, which produces code and carrier phase measurements from tracking 5G New Radio Positioning Reference Signal (PRS). Meanwhile, to handle the clock error between 5G receiver and transmitter, a round-trip time (RTT) ranging method is proposed to provide accurate 5G code-phase based range estimate using 5G PRS, and RTT method avoids clock error estimation or compensation. Then, a 5G/GNSS integrated positioning framework is proposed to combine GNSS pseudo-range measurements with 5G code-phase based range estimates. Experiments are presented of a ground platform positioning with the 5G/GNSS software defined radio transceivers, and the experimental results show that 5G/GNSS integrated positioning improves the standalone GNSS solution in terms of accuracy and availability. Meanwhile, the proposed 5G RTT ranging method shows maximum range root mean square error (RMSE) of 1.109 m.

I. INTRODUCTION

The global navigation satellite system (GNSS) is capable of providing accurate position and time estimates in ideal line-of-sight (LOS) conditions. However, the GNSS signals are weak in non-line-of-sight (NLOS) environments, such as urban canyons and

 https://doi.org/10.33012/2022.18389

indoor areas, where it is very challenging or impossible for GNSS alone to provide accurate positioning due to the lack of reliable observable. On the other hand, as the successor of Long-Term Evolution (LTE), the fifth generation (5G) is focused on three main application areas: Enhanced Mobile Broadband, Ultra Reliable Low Latency Communications, and Massive Machine Type Communications. The 5G enhances LTE in terms of bandwidth, latency, frequency resource, these features along with multiple-input-multiple-output (MIMO) and millimeter wave (mmWave) make 5G positioning attract considerable attention in recent years. In the Rel-17, 3GPP (2022) Technical Specification (TS) 38.305 concludes supported 5G positioning methods, which include, but not limited to, network-assisted GNSS, multi-round trip time positioning, angle-based positioning and time difference of arrival (TDoA) positioning using New Radio (NR) signals. The emergence of 5G positioning provides a promising opportunity to augment GNSS in some challenging environments, thereby improving stand-alone GNSS performance in terms of positioning accuracy and availability.

In terms of LTE/5G standalone positioning, Yang et al. (2000) adopt a delay-locked loop (DLL) to solve the timing recovery and pilot symbol timing estimation problems in orthogonal frequency division multiplexing (OFDM) system. Orabi et al. (2021) propose a time-delay neural network (TDNN), which achieves ranging root mean square error (RMSE) reduction of 27.1% compared to a conventional DLL through simulations. Shamaei et al. (2016) propose a LTE software defined radio (SDR), which is able to obtain robust time of arrival (ToA) estimate, and experimental results show a mean distance difference of 11.96 m against the Global Positioning System (GPS) solutions. Some improvements, e.g. clock error estimation, are made by Shamaei et al. (2018). Shamaei and Kassas (2018) also use a phase-locked loop (PLL)-aided DLL to track the received LTE signals, a position RMSE of 3.17 m is observed. Abdallah et al. (2020) assess 5G signal for opportunistic navigation, a position RMSE of 14.9 m is observed by using 5G Synchronization Signal (SS) from two 5G base stations (referred to as gNodeBs). Jin et al. (2021) evaluate ranging performance using dedicated 5G NR Positioning Reference Signal (PRS), and the simulation results show that the mean of ranging errors is 1.27 m. Chen et al. (2021) propose a carrier phase ranging method that uses 5G Physical Broadcast Channel (PBCH) Demodulation Reference Signal (DM-RS) to estimate ToA, the probability of range accuracy within 0.8 m is 95% over a trajectory of less than 10 m. Meanwhile, Abdallah and Kassas (2021) also propose a 5G SDR using 5G PBCH DM-RS for phase tracking and carrier phase measurements, the position RMSE over a trajectory of 500 m is 3.35 m. In these ToA based positioning/ranging methods, clock error among transceivers will have to be estimated and compensated, since the clock error accumulating over time results in increasing positioning error.

The development of 5G positioning techniques paves the way for integrating 5G signal with GNSS in order to further improve positioning accuracy and availability. In GINTO5G project, Mata et al. (2020) adopt Sounding Reference Signal (SRS) and combine corresponding 5G ToAs with GNSS pseudo-range measurements, but there is no significant performance improvement when 5G ToAs are incorporated in selected test sites. Moreover, a common clock is used to synchronize Universal Software Radio Peripheral (USRP)-emulated gNodeBs, so that the TDoA measurements do not incorporate clock error, which may not be feasible in practical 5G networks. However, it also points out that their early evaluation indeed shows that the hybrid approach has the potential for optimizations, resulting in an overall increased accuracy for combined 5G and GNSS. Meanwhile, Tobie et al. (2020) hybrid 5G ToA measurements deriving from 5G SS and PBCH with GNSS pseudo-range measurements, the simulation results show an improved positioning accuracy compared with standalone navigation solutions. Renaudin et al. (2021) provide a general framework for the numerical computation of the Cramér-Rao Lower Bound (CRLB) for 5G ToA estimation, the simulation results using 5G Channel State Information Reference Signal (CSI-RS) show potential sub-meter positioning accuracy with 5 gNodeBs deployed. Through simulations, Fabius et al. (2021) integrate GNSS pseudo-range measurements with 5G TDoA and Angle of Departure (AoD), the experimental results show m-level positioning accuracy with significant accuracy improvements compared to standalone 5G or GNSS positioning. To avoid the accumulated clock error in TDoA measurements, Yin et al. (2018) propose a novel 5G/GNSS integrated positioning scheme using 5G device to device (D2D) communication networks, a crossover multiple-way ranging protocol is proposed, and the simulation results that integrating 5G D2D measurements with GNSS reduces the GNSS position RMSE from around 5 m to 3 m. del Peral-Rosado et al. (2020) adopt round-trip time (RTT) measurements to integrate with GNSS pseudo-range, the simulation results indicate that adding only one 5G RTT measurement to the GNSS observables significantly improves the positioning performance, if high-accuracy 5G RTT measurement with a 1-m standard deviation is applied, the horizontal positioning accuracy of 10m on the 80% of cases is achievable.

This paper investigates integrating GNSS with 5G RTT measurements, and it makes the following contributions:

1. 5G NR PRS is introduced to be reference signals of the proposed 5G code and carrier phase receiver. In which, dedicated path time delay estimation method and DLL for 5G PRS are developed.
2. It develops a 5G/GNSS integrated positioning method, which augments GNSS pseudo-range measurements with one 5G RTT measurement.
3. To avoid estimating clock error, a RTT ranging method is implemented. The experimental results demonstrate accurate 5G RTT measurement is possible. It implements the proposed 5G SDR transceiver and integrated solution on a universal platform, actual data is collected, it then assesses integrated positioning performance using 5G SS and PRS.

The remainder of the paper is organized as follows. Section II describes 5G signals used for positioning purposes. Section III presents a dedicated 5G SDR transceiver for 5G PRS. Section IV proposes a 5G/GNSS integrated positioning solution using 5G RTT measurement and GNSS pseudo-range measurements. Section V demonstrates the experimental results. Conclusions are drawn in Section VI.

II. 5G NR SIGNAL FRAME AND SIGNALS

1. Signal Frame Structure and Numerology

5G NR can operate in the frequency ranges FR1 (410 MHz $\sim$ 7125 MHz) and FR2 (24250 MHz $\sim$ 52600 MHz). 5G NR adopts OFDM modulation, and a cyclic prefix (CP) is inserted in the OFDM symbol to combat intersymbol interference (ISI) in a multipath channel. An example frame structure is given in Fig. 1a. In the time domain, signal transmissions are organized into frames with 10 ms duration, each consisting of 10 subframes, and there are $N^{\text{slot}}_{\text{symb}} \in \{1, 2, 4, 8, 16\}$ slots in a subframe with 14 consecutive OFDM symbols in one slot for normal CP. In the frequency domain, flexible subcarrier spacing (SCS), $\Delta f = 2^{\mu} \cdot 15$ kHz where $\mu \in \{0, 1, 2, 3, 4\}$, is supported. The smallest physical resource in 5G is the Resource Element (RE), given by one subcarrier in the frequency domain and one OFDM symbol in the time domain. A Resource Block (RB) consists of 12 consecutive subcarriers in the frequency domain. Physical signals, e.g. PRS, are transmitted via signal frame with OFDM symbols occupying corresponding REs.

2. Synchronization Signal/PBCH Block (SSB)

Cell search is the procedure for a user equipment (UE) to acquire time and frequency synchronization with a cell and to detect the physical layer Cell ID of the cell. A UE receives SS consisting of Primary Synchronization Signal (PSS) and Secondary Synchronization Signal (SSS) in order to perform cell search. As shown in Fig. 1b, PSS and SSS occupies 1 OFDM symbol and 127 subcarriers, and PBCH spans across 3 OFDM symbols and 240 subcarriers. A UE assumes that reception occasions of a SS/PBCH block (SSB) are in 4 consecutive symbols with a few SSBs form one SS Burst, and SS Burst is used during beam sweeping by changing beam direction of each SSB. A set of SS Bursts is referred to as an SS Burst Set, the maximum number of SSBs in an SS Burst is frequency-dependent and it can be 4, 8, 64. The SS burst set periodicity is default at 20 ms, which is four times longer than that in LTE (5 ms) aiming at reducing the "always-on" transmission overheads.

There are 1008 unique physical-layer cell identities given by

$$N^{\text{cell}}_{\text{ID}} = 3N^{(1)}_{\text{ID}} + N^{(2)}_{\text{ID}}, \tag{1}$$

where $N^{(1)}_{\text{ID}} \in \{0, 1, \ldots, 335\}$ and $N^{(2)}_{\text{ID}} \in \{0, 1, 2\}$. PSS is a Binary Phase-shift keying (BPSK) modulated m-sequence of length 127 generated with $N^{(2)}_{\text{ID}}$. SSS is a BPSK modulated Gold sequence of length 127 generated by using $N^{(1)}_{\text{ID}}$ and $N^{(2)}_{\text{ID}}$. Hence, PSS and SSS together are used to indicate a total of (336×3) different physical physical cell identities.

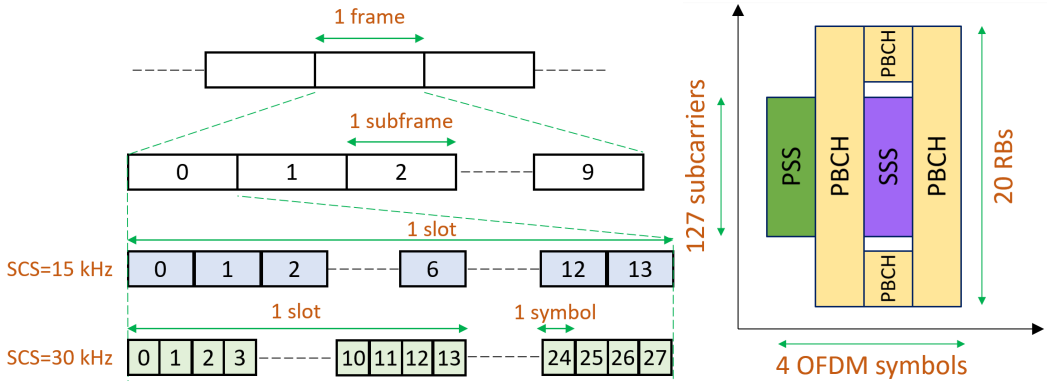

(a) Example of 5G NR frame structure **(b)** Time-frequency Structure of SSB

Figure 1: 5G NR Signal Frame

3. NR Positioning Reference Signal

A PRS sequence, $r(m)$ where $m = 0, 1, \ldots$, is a pseudo-random Quadrature Phase-shift keying (QPSK) sequence, each element of which is configured in one RE (k, l), where k is the index in the frequency domain and l refers to the symbol position in

the time domain relative to a reference point. Thus, for each Downlink (DL) PRS resource configured, the value, $\alpha_{k,l}$, of a RE (k, l) is given by

$$\alpha_{k,l} = \beta_{\text{PRS}} r(m), \tag{2}$$

$$k = mK_{\text{comb}}^{\text{PRS}} + \left[(k_{\text{offset}}^{\text{PRS}} + k') \mod K_{\text{comb}}^{\text{PRS}}\right], \tag{3}$$

$$l = l_{\text{start}}^{\text{PRS}}, l_{\text{start}}^{\text{PRS}} + 1, \ldots, l_{\text{start}}^{\text{PRS}} + L_{\text{PRS}} - 1, \tag{4}$$

where $K_{\text{comb}}^{\text{PRS}}$ denotes comb size, $k_{\text{offset}}^{\text{PRS}}$ is resource-element offset, L_{PRS} represents the size of the DL PRS resource in the time domain, $l_{\text{start}}^{\text{PRS}}$ is the first symbol of the DL PRS within a slot, and they are all given by the higher-layer parameters while β_{PRS} is a scale factor, and quantity k' is given by 3GPP (2021a).

A positioning frequency layer consists of one or more DL PRS resource sets, each of which consists of one or more DL PRS resources as described in 3GPP (2021b). The UE assumes that the parameters shown in Fig. 2a for DL PRS resources are configured via higher layer parameters DL-PRS-PositioningFrequencyLayer, DL-PRS-ResourceSet and DL-PRS-Resource.

Suppose $K_{\text{comb}}^{\text{PRS}} = 2$, $l_{\text{start}}^{\text{PRS}} = 2$, $L_{\text{PRS}} = 2$ and $k_{\text{offset}}^{\text{PRS}} = 0$, then, we have $k' = 0, 1$, $l = 2, 3$, and k is given by

$$k = m \times 2 + [(0 + \{0, 1\}) \mod 2]. \tag{5}$$

Based on the assumptions above, an example of mapping DL PRS resources to one slot of signal frame is given by Fig. 2b, from which one can draw some conclusions with regards to the pattern of 5G NR DL PRS:

1. PRS symbols only occupy a certain number of subcarriers instead of using all subcarriers
2. PRS symbols are evenly allocated into some of subcarriers in one OFDM symbol
3. PRS symbols are diagonal across the OFDM symbols in one slot

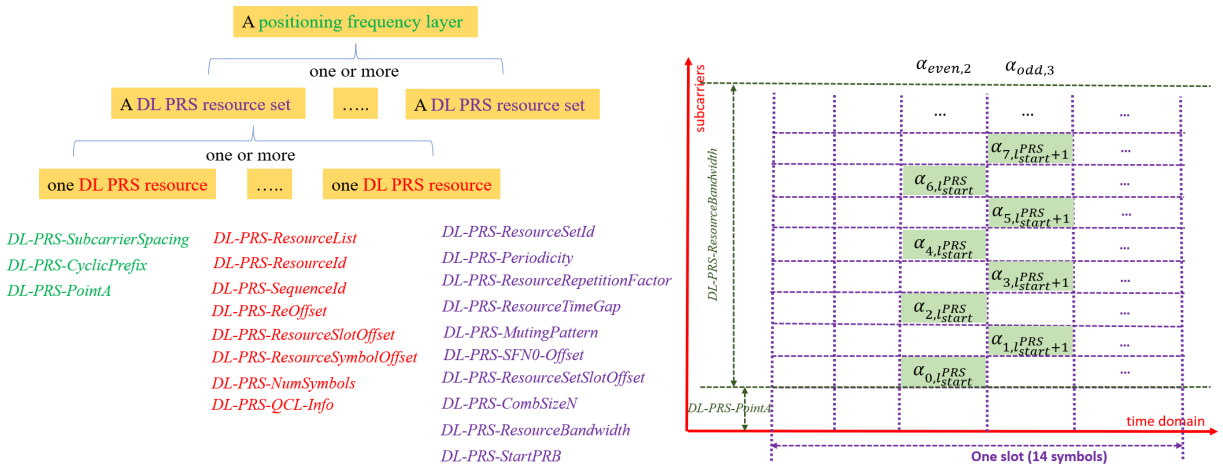

(a) NR DL Positioning Reference Signal layers

(b) Mapping DL PRS to physical resources

Figure 2: NR Positioning Reference Signal

Therefore, by the definition of a PRS sequence, one can note that the PRSs over one OFDM symbol are allocated to certain but not entire subcarriers with even spacing. Hence, as shown in Fig. 3, without loss of generality, the pattern of one PRS sequence over one OFDM symbol period is given by

$$n(m') = a\, m' + c, \tag{6}$$

$$N = a\, M + b, \tag{7}$$

where $\{n(m') | m' \in 0, 1, \ldots, M-1\}$ denotes that the m'-th reference symbol is allocated to the n-th subcarrier, N is the total number of subcarriers and we assume that N is even and equal to fast Fourier transform (FFT) size, M denotes the total symbol number of one PRS sequence in the frequency domain, a represents the subcarrier separation of two adjacent reference symbols,

and c denotes the subcarrier offset of the first reference symbol with respect to (w.r.t.) subcarrier 0, b is a known constant. Here, b and c can be different values during different OFDM symbol periods, i.e., we assume reference symbols over each OFDM symbol period follow a specific pattern. This ensures that for any particular symbol period k, where a PRS sequence exists, the pattern conforms to the definition in 3GPP (2021a).

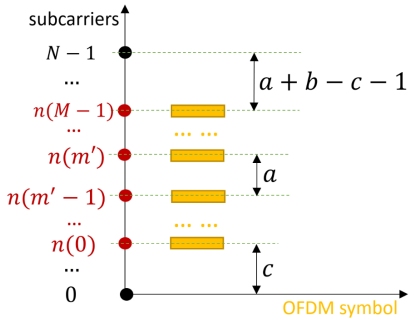

Figure 3: Pattern of Positioning Reference Signals

III. 5G CODE AND CARRIER PHASE RECEIVER

The proposed receiver is comprised of several stages: coarse signal synchronization, generalized path time delay estimate, DLL/PLL phase tracking, as shown in Fig. 4. The purpose of coarse signal synchronization is to obtain coarse symbol synchronization by cross-correlation of the received sample sequence r with the local generated reference signal sequence r_l. The generalized path time delay estimation is responsible for reducing the timing error within one sample, while the DLL and PLL dynamically estimate and track the remaining fractional timing error in a closed-loop manner. In the DLL/PLL phase tracking stage, a dedicated DLL for 5G PRS is proposed, while the PLL comprises a carrier phase discriminator, a lowpass filter (LPF) and an accumulator.

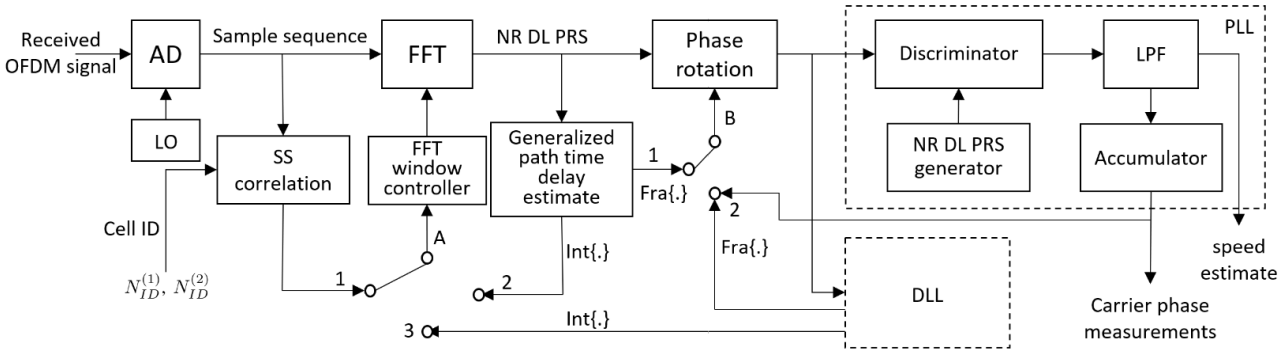

Figure 4: Block diagram of the proposed 5G code and carrier phase receiver

1. Coarse Synchronization

The purpose of coarse signal synchronization is to find the first received sample belonging to one OFDM symbol by cross-correlation. From Section II.2 one can note that PSS/SSS are generated by unique physical-layer cell identities $N_{\mathrm{ID}}^{(1)}$ and $N_{\mathrm{ID}}^{(2)}$. In this paper, PSS/SSS is adopted to complete coarse signal synchronization by cross-correlation of the received sample sequence r with the local generated PSS/SSS sequence r_l, which can be found at (Shamaei and Kassas, 2018). The PSS/SSS with the same cell ID, i.e. $N_{\mathrm{ID}}^{(1)}$ and $N_{\mathrm{ID}}^{(2)}$, as the transmitter has the peak cross-correlation value. The coarse timing offset estimate $\hat{\theta}_c$ w.r.t. sequence r is given by

$$\hat{\theta}_c \triangleq \max\{\mathrm{xcorr}_{r,r_l}[Q:(2Q-1)]\}-1, \tag{8}$$

where Q is the total sample number of r, and xcorr_{r,r_l} represents the correlation operation, it returns $(2Q-1)$ cross-correlation results of two discrete-time sequences r and r_l.

2. Generalized Path Time Delay Estimation

Define the timing error $e_\theta = \hat{\theta} - \theta_o$, where θ_o denotes the actual timing offset w.r.t. the first received sample, and $\hat{\theta}$ is the estimated timing offset. The timing offsets $\hat{\theta}$ and θ_o are normalized by the sampling interval T.

Suppose a multi-path channel with L paths as characterized in Yang et al. (2000). Let τ_l be the path propagation time delay of the l-th path, where τ_0 corresponds to the LOS path and the rest are NLOS delays. Without loss of generality, after coarse symbol synchronization, assume the residual timing error of the LOS path delay after FFT window adjustment is e_θ, where e_θ denotes the unknown timing error that needs to be estimated. The received symbol, $\widehat{X}_{k,n}$, over the k-th OFDM symbol period and on the n-th subcarrier can be written as

$$\widehat{X}_{k,n} = \sum_{l=0}^{L-1} h_l(kT_s) e^{\frac{j2\pi(n-\frac{N}{2})}{N}(e'_\theta - \tau'_l)} X_{k,n} + n_{k,n}, \tag{9}$$

where $h_l(\cdot)$ is the complex gain of the l-th path, $\tau'_l = \tau_l \mod T$, and $e'_\theta = e_\theta - \left(\frac{\tau_l}{T} - \tau'_l\right)$, $n_{k,n}$ is a white complex Gaussian noise with variance σ^2. Thus, for any transmitted reference symbol $X_{k,n(m')}$ over the k-th OFDM symbol where $n(m')$ is defined by (6) and (7), the estimated channel frequency response at each subcarrier frequency can be given by $\widehat{H}_{k,n(m')} = \frac{\widehat{X}_{k,n(m')}}{X_{k,n(m')}}$. For any $m' \in [M, 2M-1]$, let $\widehat{H}_{k,n(m')} = 0$. Applying the $2M$-point inverse fast Fourier transform (iFFT) to estimate the channel impulse response, for $m = 0, 1, \ldots, 2M-1$, it gives

$$\widehat{h}_{k,m} = \frac{1}{2M} \sum_{l=0}^{L-1} h_l(kT_s) \left(e^{j2\pi \frac{c-\frac{N}{2}}{N}(e'_\theta - \tau'_l)} \sum_{m'=0}^{2M-1} e^{j2\pi m'(\frac{a}{N}(e'_\theta - \tau'_l) + \frac{m}{2M})} \right) + n'_{k,n}. \tag{10}$$

Here, $n'_{k,n}$ is white Gaussian noise. For the additive white Gaussian noise (AWGN) or multipath Ricean fading channels, the actual timing error is assumed to be introduced by the first path time delay of the channel. Therefore, the estimated timing error $\hat{e}_\theta$ over the k-th OFDM symbol period is given by

$$\hat{e}_\theta = -\frac{\widehat{m}}{2} - \frac{b\widehat{m}}{2aM}, \tag{11}$$

where

$$\widehat{m} = \arg\max_m \sum_{j=0}^{N_{av}-1} \left| \widehat{h}_{k-j,m} \right|^2. \tag{12}$$

Similar to Yang et al. (2000), to mitigate the multi-path impact, N_{av} consecutive channel impulse responses can be averaged as described in (12). The estimation method described in this section is called the generalized path time delay estimate, because it generalizes the PRS sequence pattern determined by a, b, c, M and defined in (6) and (7), and corresponding timing error estimate is given by (11).

3. Code Phase Tracking for 5G PRS

A late-minus-early DLL can be used to track and estimate rotated phase of reference symbol $X_{k,n}$, which is derived from a PRS sequence descried in Section II.3. After the timing estimation process enters DLL tracking stage, the tracking loop will adjust received PRS symbol phase by using the estimated symbol timing error $\hat{e}_\theta$. Then, the received PRS symbols after symbol phase adjustment can be written as

$$\widehat{X}_{k,n(m)} = e^{-j2\pi \frac{am+c-\frac{N}{2}}{N}\epsilon} X_{k,n(m)} + n_{k,n}, \tag{13}$$

where $\epsilon = \hat{e}_\theta - e_\theta$ is the normalized loop tracking error, $n_{k,n}$ is a white complex Gaussian noise with variance σ^2, and $n(m)$ is the subcarrier number of the m-th PRS symbol over the k-th OFDM symbol period as described in (6). Define $c' = c - \frac{N}{2}$, then, the demodulated reference symbols can be rewritten as

$$\widehat{X}_{k,n(m)} = e^{-\frac{j2\pi(am+c')\epsilon}{N}} X_{k,n(m)} + n_{k,n}. \tag{14}$$

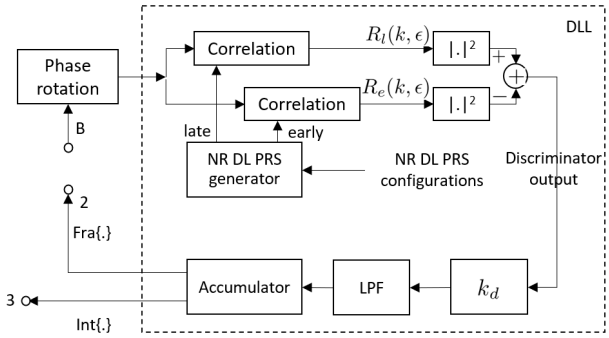

Figure 5: Block Diagram of the Delay-locked Loop

Suppose during the k-th OFDM symbol period, $|X_{k,n(m)}| = 1$. Then, for the AWGN channel, the local generated early reference symbols, $X_e(m)$, are given by

$$X_e(m) = e^{-\frac{j2\pi(am+c')\xi}{N}} X_{k,n(m)}, \tag{15}$$

where $m = 0, \ldots, M-1$, and $\{\xi | 0 < \xi \leq 0.5\}$ is the advanced (and retarded) interval normalized to the sample interval. The conjugation of (15) is given by

$$X_e^*(m) = e^{\frac{j2\pi(am+c')\xi}{N}} X_{k,n}^*. \tag{16}$$

Therefore, the early cross-correlation branch output can be given by

$$\begin{aligned} R_e(k,\epsilon) &= \sum_{m=0}^{M-1} \widehat{X}_{k,n(m)} X_e^*(m) \\ &= e^{j\frac{2\pi c'(\xi-\epsilon)}{N}} \sum_{m=0}^{M-1} e^{j\frac{2\pi am(\xi-\epsilon)}{N}} + N_e, \end{aligned} \tag{17}$$

where $N_e = \sum_{m=0}^{M-1} e^{\frac{j2\pi(am+c')\xi}{N}} X_{k,n(m)}^* n_{k,n}$. (17) can be rewritten as

$$\begin{aligned} R_e(k,\epsilon) &= e^{j\frac{2\pi c'(\xi-\epsilon)}{N}} \sum_{m=0}^{M-1} e^{j\frac{2\pi am(\xi-\epsilon)}{N}} + N_e \\ &= e^{j\phi_e} \frac{\sin(\frac{\pi a(\xi-\epsilon)M}{N})}{\sin(\frac{\pi a(\xi-\epsilon)}{N})} + N_e, \end{aligned} \tag{18}$$

where $\phi_e = \frac{2\pi c'(\xi-\epsilon)}{N} + \frac{\pi a(\xi-\epsilon)(M-1)}{N}$, and $|R_e(k,\epsilon)|^2$ is a non-central Chi-square with 2 degrees of freedom, its mean and variance are

$$\mathbb{E}[|R_e(k,\epsilon)|^2] = \frac{\sin(\frac{\pi a(\xi-\epsilon)M}{N})}{\sin(\frac{\pi a(\xi-\epsilon)}{N})} + M\sigma^2, \tag{19}$$

$$\mathrm{Var}[|R_e(k,\epsilon)|^2] = M^2\sigma^4 \left[1 + \frac{2}{M\sigma^2} \left(\frac{\sin(\frac{\pi a(\xi-\epsilon)M}{N})}{\sin(\frac{\pi a(\xi-\epsilon)}{N})} \right)^2 \right]. \tag{20}$$

Similarly, the local generated late reference symbols are given by

$$R_l(k,\epsilon) = e^{j\phi_l} \frac{\sin(\frac{\pi a(\xi+\epsilon)M}{N})}{\sin(\frac{\pi a(\xi+\epsilon)}{N})} + N_l, \tag{21}$$

where $\phi_l = \frac{2\pi c'(-\xi-\epsilon)}{N} - \frac{\pi a(\xi+\epsilon)(M-1)}{N}$, and $|R_l(k,\epsilon)|^2$ is a non-central Chi-square with 2 degrees of freedom, its mean and variance are

$$\mathbb{E}[|R_l(k,\epsilon)|^2] = \frac{\sin(\frac{\pi a(\xi+\epsilon)M}{N})}{\sin(\frac{\pi a(\xi+\epsilon)}{N})} + M\sigma^2, \tag{22}$$

$$\mathrm{Var}\left[|R_l(k,\epsilon)|^2\right] = M^2\sigma^4 \left[1 + \frac{2}{M\sigma^2}\left(\frac{\sin(\frac{\pi a(\xi+\epsilon)M}{N})}{\sin(\frac{\pi a(\xi+\epsilon)}{N})}\right)^2\right]. \tag{23}$$

Hence, the normalized S-curve function, $S(\epsilon,\xi)$, is given by

$$\begin{aligned} S(\epsilon,\xi) &= \mathbb{E}\left[\frac{|R_l(i,\epsilon)|^2 - |R_e(i,\epsilon)|^2}{M^2}\right] \\ &= \frac{\left|e^{j\phi_l}\frac{\sin(\frac{\pi a(\xi+\epsilon)M}{N})}{\sin(\frac{\pi a(\xi+\epsilon)}{N})}\right|^2 - \left|e^{j\phi_e}\frac{\sin(\frac{\pi a(\xi-\epsilon)M}{N})}{\sin(\frac{\pi a(\xi-\epsilon)}{N})}\right|^2}{M^2}. \end{aligned} \tag{24}$$

The partial derivative $\frac{\partial}{\partial\epsilon}S(\epsilon,\xi)$ is described in (25). In addition, when $\epsilon = 0$, (25) can be given by (26).

$$\begin{aligned} \frac{\partial}{\partial\epsilon}S(\epsilon,\xi) &= \frac{2}{M^2}\left(\frac{\sin(\frac{\pi a(\epsilon+\xi)M}{N})}{\sin(\frac{\pi a(\epsilon+\xi)}{N})}\right)\left(\frac{\sin(\frac{\pi a(\epsilon+\xi)M}{N})}{\sin(\frac{\pi a(\epsilon+\xi)}{N})}\right)' - \frac{2}{M^2}\left(\frac{\sin(\frac{\pi a(\epsilon-\xi)M}{N})}{\sin(\frac{\pi a(\epsilon-\xi)}{N})}\right)\left(\frac{\sin(\frac{\pi a(\epsilon-\xi)M}{N})}{\sin(\frac{\pi a(\epsilon-\xi)}{N})}\right)' \\ &= \frac{2}{M^2}\frac{\pi a}{N}\left(\frac{M\sin(\frac{\pi a(\epsilon+\xi)M}{N})\cos(\frac{\pi a(\epsilon+\xi)M}{N})\sin(\frac{\pi a(\epsilon+\xi)}{N}) - \sin(\frac{\pi a(\epsilon+\xi)M}{N})\sin(\frac{\pi a(\epsilon+\xi)M}{N})\cos(\frac{\pi a(\epsilon+\xi)}{N})}{\left[\sin(\frac{\pi a(\epsilon+\xi)}{N})\right]^3}\right) \\ &\quad - \frac{2}{M^2}\frac{\pi a}{N}\left(\frac{M\sin(\frac{\pi a(\epsilon-\xi)M}{N})\cos(\frac{\pi a(\epsilon-\xi)M}{N})\sin(\frac{\pi a(\epsilon-\xi)}{N}) - \sin(\frac{\pi a(\epsilon-\xi)M}{N})\sin(\frac{\pi a(\epsilon-\xi)M}{N})\cos(\frac{\pi a(\epsilon-\xi)}{N})}{\left[\sin(\frac{\pi a(\epsilon-\xi)}{N})\right]^3}\right), \end{aligned} \tag{25}$$

$$\frac{\partial}{\partial\epsilon}S(\epsilon,\xi=0.5)|_{\epsilon=0} = \frac{4\pi a}{NM^2}\left(\frac{M\sin(\frac{\pi aM}{2N})\cos(\frac{\pi aM}{2N})\sin(\frac{\pi a}{2N}) - \sin(\frac{\pi aM}{2N})\sin(\frac{\pi aM}{2N})\cos(\frac{\pi a}{2N})}{\left[\sin(\frac{\pi a}{2N})\right]^3}\right). \tag{26}$$

In contrast, Yang et al. (2000); Chen et al. (2015, 2016, 2021); Shamaei and Kassas (2018); Abdallah et al. (2019) either assume $b = 0$, $c = 0$ or $[2\,c + a(M-1)]/N \approx 1$. For instance, Yang et al. (2000) assume $b = c = 0$, then based on (7) it gives $N = aM$, therefore, (26) is downgraded to

$$\frac{\partial}{\partial\epsilon}S(\epsilon,\xi=0.5)|_{\epsilon=0} = \frac{4\pi}{M^3}\frac{-\cos(\frac{\pi}{2M})}{\left[\sin(\frac{\pi}{2M})\right]^3}. \tag{27}$$

(27) is identical to Eq. (40) of Yang et al. (2000). It indicates that in the DLL for tracking 5G PRS, a specific slope estimate of the normalized S-curve function for generalized 5G PRS pattern is required. After timing error estimation, a low-pass filter is applied to smooth the discriminator output, and an accumulator is used to integrate the estimation.

To sum up, for any given 5G PRS pattern defined in (6) and (7), we present corresponding normalized S-curve function slope estimate described in (26), hence, during the estimation process no approximation or additional assumption in terms of the pattern of reference symbols is required. The inaccurate slope estimate may result in longer loop convergence time, which may not be feasible in real-time applications.

IV. A 5G/GNSS INTEGRATED POSITIONING FRAMEWORK

1. Round-trip Time Ranging

In the standard RTT method, device B in Fig. 6 needs to precisely estimate the ToA of a ranging marker (RMARKER), i.e. 5G PRS, it then feeds back the response signal after a certain delay T_{reply}. Estimating the ToA and maintaining accurate timing control on device B requires complex implementation in practice.

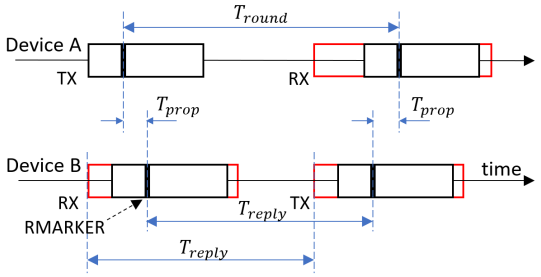

Figure 6: RTT Ranging

To avoid the difficulties mentioned above, our proposed method defines new transmission and reception windows in the RTT ranging process. As shown in Fig. 6, black rectangles represent the actual signal of arrival, while the new proposed transmission/reception window is indicated by a red rectangle, which is sufficiently large so that it is guaranteed to contain the transmitted reference symbol represented by RMARKER. Device B records the signal (including noise) received within its reception window and simply re-transmits it after a fixed delay T_{reply}. Therefore, there is no need to perform a ToA estimation at device B, because device B's transmission delay is equal to RMARKER's transmission delay T_{reply} as shown in Fig. 6. On the other hand, device A's reception window has to be sufficiently large to receive the re-transmitted signal from device B. Device A performs a ToA estimation to determine time of arrival of the RMARKER.

From device A's perspective, define that during the k-th ranging period, $r[k]$ denotes the range between device A and B, and corresponding ToA estimate of PRS is $\mathrm{S}_a[k]$, which is normalized by the sampling interval T. If $r[0]$ and $\mathrm{S}_a[0]$ are known to device A at a calibration stage, then, during the k-th ranging period, the estimated range $\hat{r}[k]$ can be given by

$$\begin{aligned}\hat{r}[k] &= \frac{1}{2}(T_{\text{round}}[k]\text{-}T_{\text{reply}}[k]\text{-}(T_{\text{round}}[0]\text{-}T_{\text{reply}}[0])\text{+}2r[0]) \\ &\approx \frac{1}{2}\alpha(\mathrm{S}_a[k]-\mathrm{S}_a[0])+r[0],\end{aligned} \tag{28}$$

where T_{round} is RMARKER's round-trip time including T_{reply} introduced by device B, $\alpha = c_l\, T$ denotes the distance in meters one sample represents, and c_l is the speed of light in vacuum. In (28), the calibration period 0 requires knowledge of the actual range $r[0]$. This corresponds to a site or in-lab calibration before the ranging period k. The error in the range estimate (28) can be bounded as

$$|\Delta r[k]| \leq \frac{c_l T_{\text{reply}}}{2}(2e_e + e_g), \tag{29}$$

where e_e and e_g are device A and B's maximum clock frequency offset w.r.t. the standard clock, respectively. In our case, T_{reply} is 267.1 ms and the nominal frequency accuracy of NI's USRP 2954R GPS-disciplined oscillator (GPSDO) is 5 ppb. From (29), the maximum range estimation error is 0.601 m.

2. 5G/GNSS Fusion

To integrate 5G with GNSS signal, we augment GNSS pseudo-range measurements with 5G range measurements provided by the proposed 5G code and carrier-phase receiver. Suppose there are N_s GNSS satellites available and one 5G measurement, then, the pseudo-range measurements can be given by

$$\begin{cases} \rho_c^{(1)} & = \rho^{(1)} + \delta t_u + \varepsilon^{(1)} \\ \rho_c^{(2)} & = \rho^{(2)} + \delta t_u + \varepsilon^{(2)} \\ & \dots \\ \rho_c^{(N_s)} & = \rho^{(N_s)} + \delta t_u + \varepsilon^{(N_s)} \\ \hat{r} & = \rho^{(5\mathrm{G})} + \varepsilon^{(5\mathrm{G})}, \end{cases} \tag{30}$$

where $\{\rho_c^{(i)} | i = 1, 2, \dots, N_s\}$ denotes the i-th satellite's pseudo-range measurement, $\rho^{(i)}$ is the range between the i-th satellite and GNSS receiver, δt_u is GNSS receiver clock offset w.r.t. GPS time in meters, and $\varepsilon^{(i)}$ includes receiver noise and all the rest error terms associated with the i-th satellite. $\hat{r}$ represents the 5G range estimate given by (28), $\rho^{(5\mathrm{G})}$ denotes the range between gNodeB and 5G receiver on the UE end, $\varepsilon^{(5\mathrm{G})}$ includes 5G receiver measurement noise and all other error terms. Here, it assumes gNodeB's position is known to the UE, the antennas of 5G receiver and GNSS receiver are placed together.

Based on (30), the UE's position, (x, y, z), can be determined via a weighted least squares (WLS) solution. That is, during the k-th iteration of Newton's method, the unknown parameter vector $\mathbf{x}$ is given by

$$\mathbf{x} = \mathbf{x}_{k-1} + \Delta\mathbf{x}, \tag{31}$$

where

$$\mathbf{x} = \begin{bmatrix} x \\ y \\ z \\ \delta t_u \end{bmatrix}, \tag{32}$$

$$\Delta\mathbf{x} = (\mathbf{G}^{\mathrm{T}}\mathbf{C}\mathbf{G})^{-1}\mathbf{G}^{\mathrm{T}}\mathbf{C}\mathbf{b}, \tag{33}$$

$$\mathbf{C} = \mathbf{W}^{\mathrm{T}}\mathbf{W}, \tag{34}$$

$$\mathbf{W} = \begin{bmatrix} \sigma_S^{-1} & & & \\ & \sigma_S^{-1} & & \\ & & \dots & \\ & & & \sigma_{5G}^{-1} \end{bmatrix}, \tag{35}$$

and $\mathbf{G}$ denotes Jacobian matrix, $\mathbf{b}$ is residual vector of dimension $N_s + 1$, $\mathbf{W}$ is the observation weight matrix, σ_S and σ_{5G} are the standard deviations of GNSS pseudo-range and 5G measurement noise, respectively.

If there are sufficient GNSS observations, the additional 5G range measurement will enhance the GNSS-based positioning accuracy. Moreover, if the GNSS observations are insufficient, for instance, when there are less than four LOS satellites in some GNSS-challenged environments, the 5G range measurement plays the role of a pseudo-satellite, allowing the UE's position to be jointly determined by the 5G and GNSS receiver. This yields a continuous and robust positioning solution in some GNSS-challenged environments.

V. EXPERIMENTS AND RESULTS

1. Experiments for 5G RTT Ranging

In this section, we first evaluate the ranging performance by applying proposed generalized path time delay estimation and the DLL timing error tracking methods with 5G PRS. The 5G RTT ranging experiments include static experiments (see Fig. 7) in the corridor and dynamic ones on the roof of EEE building, Nanyang Technological University (NTU), Singapore. The hardware platform is NI's USRP 2954R with GPSDO, the gNodeB is placed still during the entire test. The update rate of 5G range estimate is 1 Hz.

In the static experiments, the UE is placed in five fixed points, and its relative distance w.r.t. gNodeB is 4 m, 8 m, 12 m, 16 m, 20 m, respectively. The RTT range estimation results are shown in Fig. 8a. During each second only one frame 5G signal is transmitted, and at each fixed point 120 measurements are collected on the UE end, so there are 600 measurements in total. The

mean and standard deviation of ranging error are 0.319m and 0.375m, respectively, corresponding range RMSE is 0.492 m. In the 5G RTT dynamic experiments, UE is moving towards and backwards the fixed gNodeB, corresponding ranging errors are shown in Fig. 9 with Real-Time Kinematic (RTK) Fixed solution as ground truth. The resulting range RMSE of two tests are 1.109 m and 0.997 m, respectively. From Figs. 8b and 9, one can note that there is a small offset between 5G RTT estimate and the ground truth, that is caused by (29).

Figure 7: 5G RTT Ranging in the Corridor (Static Experiments)

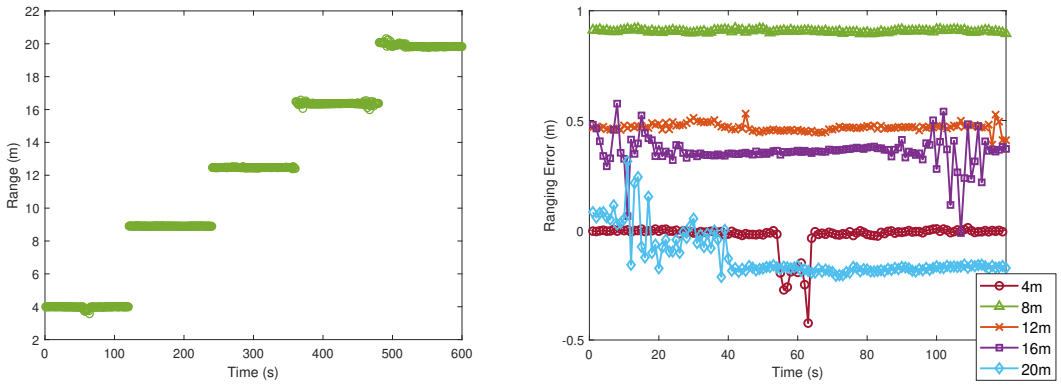

(a) RTT estimate **(b)** Ranging error

Figure 8: 5G RTT Ranging Performance in Static Experiments

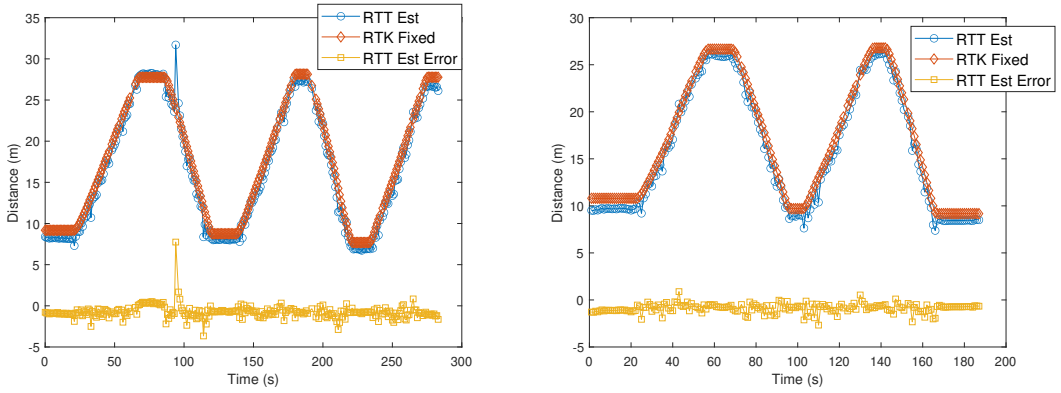

(a) 5G Dynamic Ranging - test 1 **(b)** 5G Dynamic Ranging - test 2

Figure 9: 5G RTT Ranging Performance in Dynamic Experiments

2. Experiments for 5G/GNSS Integrated Positioning

In this section, we experimentally evaluate the positioning performance of the 5G/GNSS integrated solution in the context of 5G RTT ranging. The proposed 5G receiver is implemented in a simplified 5G network using a SDR system using NI's USRP 2954R with GPSDO as the transceiver frontend. As shown in Fig. 10, the UE consists of a GNSS receiver and a 5G receiver. Meanwhile, a gNodeB is placed at a fixed position together with a GNSS receiver, which serves as a base station. In the experiments, the 5G range measurement noise standard deviation is set to be 1 m, while that of GNSS is 5 m. The 5G signal are generated and processed using the proposed 5G dedicated receiver, and the integrated positioning solution is then implemented in MATLAB.

In the 5G/GNSS integrated positioning experiment, the actual distance between the UE and gNodeB is 22.285 m. During the test, GPS pseudo-range measurements are collected from ublox C099-F9P GNSS receiver on the UE end, the UE also obtains 5G range measurements with an update rate of 1 Hz.

In the experiment, we consider only the GPS. There are a total of nine GPS satellites that can be observed. By using the pseudo-range measurements from these nine GPS satellites, a standalone pseudo-range positioning solution yields position RMSE of 3.717 m. The corresponding GPS single point positioning (SPP) error in NED frame is shown in Fig. 11a.

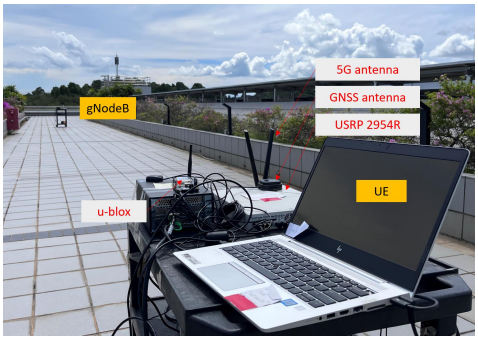

Figure 10: Experimental Setup

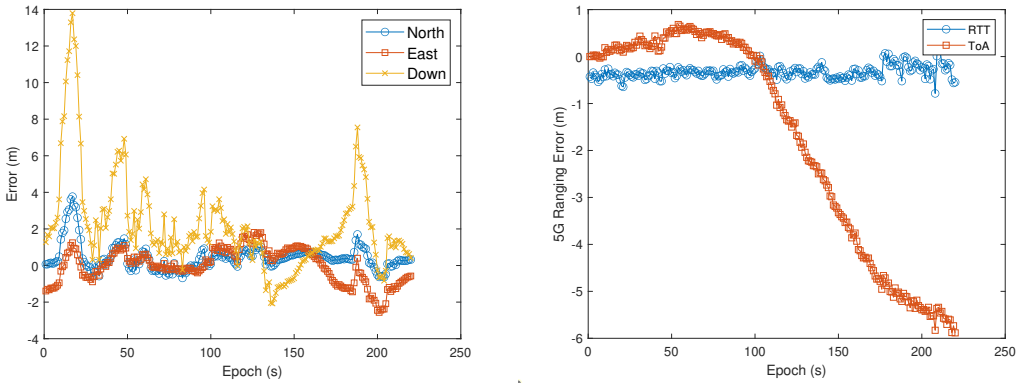

(a) GPS SPP error

(b) 5G RTT/ToA ranging error

Figure 11: Standalone Positioning Error

Besides GPS measurements, the gNodeB-UE pair also provides one 5G range estimate. The 5G ToA measurement represents the time of arrival of 5G PRS transmitted from gNodeB end and estimated on the UE end, while RTT measurement denotes the round-trip time estimate of 5G PRS between gNodeB and UE. From Fig. 11b, the experimental results show that the mean and standard deviation of 5G RTT ranging error are 0.327 m and 0.138 m, respectively, and corresponding range RMSE is 0.355 m. No site calibration is required here for RTT measurements, and in-lab calibration conducted on a separate day is sufficient to enable accurate 5G RTT range measurements. In contrast, the 5G ToA ranging error mean and standard deviation are 1.785 m and 2.327 m, respectively, and corresponding range RMSE is 2.929 m. Due to the accumulated clock error, the ToA ranging error increases over time, while RTT ranging provides stable range estimate.

During the testing epochs, the geometry of GPS satellites and 5G base station is shown in Fig. 12a. Augmenting GPS pseudo-

range measurements with 5G RTT measurement using integrated solution described in Section IV.2, the positioning error is shown in Fig. 12b, and corresponding position RMSE is 1.798 m.

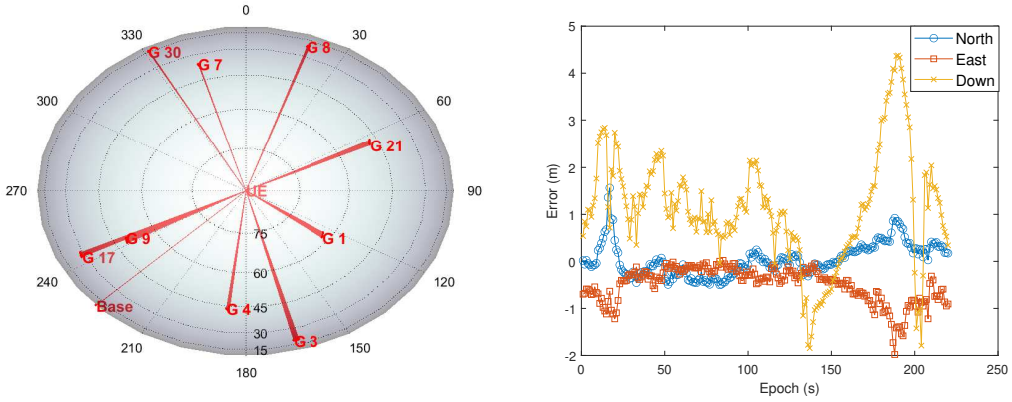

(a) Geometry of all available GPS satellites and 5G base

(b) GPS SPP/RTT 5G integrated positioning error

Figure 12: 5G/GPS Integrated Positioning

If we assume that there are only three GPS measurements available, with the assistance of one 5G range measurement, an accurate position estimation is still possible. For example, if we consider only the GPS satellites G1, G3, G30 together with one 5G RTT measurement, the resultant position RMSE is 0.846 m. As shown in Figs. 13a and 13b, with a good geometry, the 5G/GNSS integrated positioning can provide more accurate position estimate than GNSS standalone solution.

If the geometry is poor, and availability of GNSS is limited, for instance in urban canyon only few satellites are available for GNSS receiver, as shown in Fig. 14a, only G4, G9 and G17 are available and these three satellites are orbited in a similar area in terms of azimuth and elevation angle, by adding one additional 5G RTT measurement, the experimental result (see Fig. 14b) shows that position RMSE is 8.636 m.

The cumulative distribution functions (CDFs) of positioning errors are shown in Fig. 15, while positioning errors of a variety of integrated solutions are concluded in Table 1. The experimental results reveal that RTT-based 5G measurement is more accurate than the ToA-based one. In addition, integrating GNSS with only one accurate 5G measurement can improve the performance of GNSS in terms of accuracy and availability.

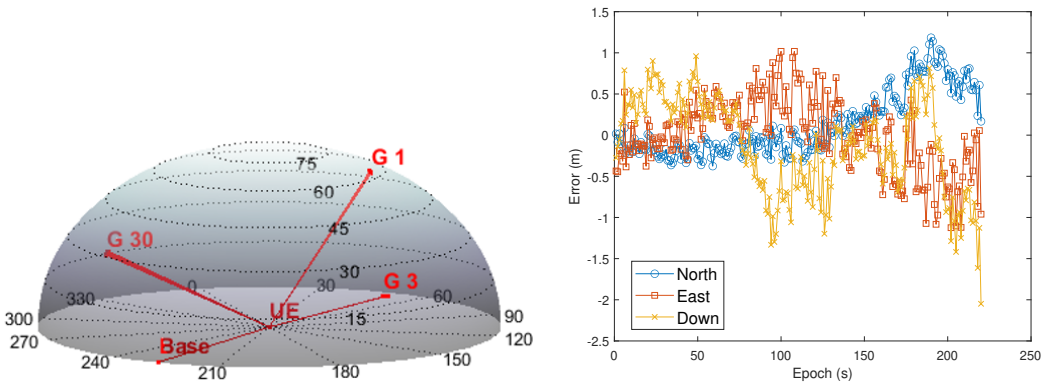

(a) Geometry of G1, G3, G30 and 5G base

(b) GPS(G1,G3,G30)/RTT 5G integrated positioning

Figure 13: 5G/GPS Integrated Positioning (good geometry)

VI. CONCLUSION

We have developed a 5G code and carrier phase receiver to obtain 5G ToA measurements. Using a RTT ranging method, accurate 5G range estimates are possible. In the dynamic experiments, the proposed 5G RTT ranging method shows that the maximum range RMSE is 1.109 m. We then integrate the 5G range estimates with GNSS pseudo-ranges and propose a

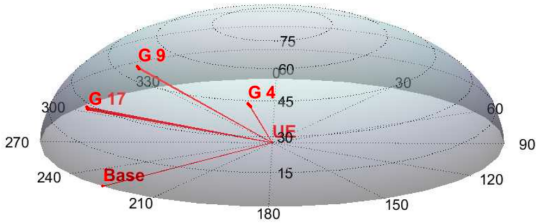

(a) Geometry of G4, G9, G17 and 5G base

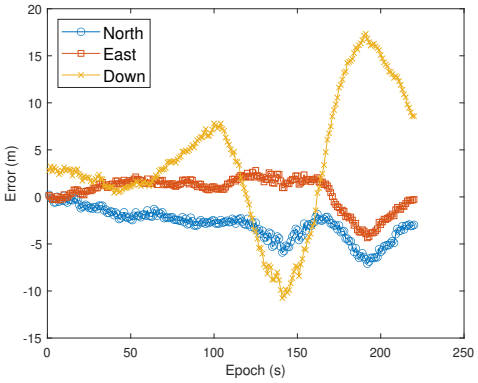

(b) GPS(G4,G9,G17)/RTT 5G integrated positioning

Figure 14: 5G/GPS Integrated Positioning (poor geometry)

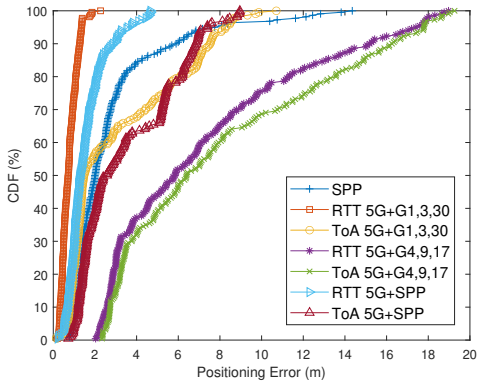

Figure 15: Cumulative Distribution Function of Positioning Errors

Table 1: Summary of Positioning Errors

	SPP	RTT+SPP	ToA+SPP	RTT+G1,G3,G30	ToA+G1,G3,G30	RTT+G4,G9,G17	ToA+G4,G9,G17
mean (m)	2.809	1.537	3.528	0.764	3.124	7.214	8.060
std (m)	2.440	0.936	2.291	0.365	2.700	4.759	5.097
RMSE (m)	3.717	1.798	4.203	0.846	4.125	8.636	9.530

WLS fusion to obtain the UE's position estimate. Experiments demonstrate that the 5G/GNSS integrated positioning method improves the standalone GNSS solution in terms of accuracy and availability. This paper paves the way for integrating GNSS with 5G to improve the performance of standalone GNSS in some GNSS-challenged environments.

ACKNOWLEDGEMENTS

This research is supported by A*STAR under its RIE2020 Advanced Manufacturing and Engineering (AME) Industry Alignment Fund – Pre Positioning (IAF-PP) (Grant No. A19D6a0053).

REFERENCES

3GPP (2021a). NR; physical channels and modulation (Release 16). TS 38.211, 3rd Generation Partnership Project (3GPP). V16.7.0.

3GPP (2021b). NR; physical layer procedures for data (Release 16). TS 38.214, 3rd Generation Partnership Project (3GPP). V16.7.0.

3GPP (2022). NG Radio Access Network (NG-RAN); Stage 2 functional specification of User Equipment (UE) positioning in NG-RAN (Release 17). TS 38.305, 3rd Generation Partnership Project (3GPP). V17.0.0.

Abdallah, A., A., Shamaei, Kimia, Kassas, and M, Z. (2020). Assessing real 5G signals for opportunistic navigation. In *Proceedings of the 33rd International Technical Meeting of the Satellite Division of The Institute of Navigation (ION GNSS+ 2020)*, pages 2548–2559.

Abdallah, A. A. and Kassas, Z. M. (2021). UAV navigation with 5G carrier phase measurements. In *Proceedings of the 34th International Technical Meeting of the Satellite Division of The Institute of Navigation (ION GNSS+ 2021)*, pages 3294–3306.

Abdallah, A. A., Shamaei, K., and Kassas, Z. M. (2019). Performance characterization of an indoor localization system with LTE code and carrier phase measurements and an IMU. In *2019 International Conference on Indoor Positioning and Indoor Navigation (IPIN)*, pages 1–8.

Chen, L., Julien, O., Thevenon, P., Serant, D., Peña, A. G., and Kuusniemi, H. (2015). TOA estimation for positioning with DVB-T signals in outdoor static tests. *IEEE Transactions on Broadcasting*, 61(4):625–638.

Chen, L., Thevenon, P., Seco-Granados, G., Julien, O., and Kuusniemi, H. (2016). Analysis on the TOA tracking with DVB-T signals for positioning. *IEEE Transactions on Broadcasting*, 62(4):957–961.

Chen, L., Zhou, X., Chen, F., Yang, L.-L., and Chen, R. (2021). Carrier phase ranging for indoor positioning with 5G NR signals. *IEEE Internet of Things Journal*, pages 1–1.

del Peral-Rosado, J. A., Gunnarsson, F., Dwivedi, S., Razavi, S. M., Renaudin, O., López-Salcedo, J. A., and Seco-Granados, G. (2020). Exploitation of 3D City Maps for Hybrid 5G RTT and GNSS Positioning Simulations. In *ICASSP 2020 - 2020 IEEE International Conference on Acoustics, Speech and Signal Processing (ICASSP)*, pages 9205–9209.

Fabius, M., Lapeyre, D., Messager, F., Kiely, I., Arzel, L., and Pomies, A. (2021). GEONAV IoT-Study of Hybrid 5G/GNSS Positioning. In *Proceedings of the 34th International Technical Meeting of the Satellite Division of The Institute of Navigation (ION GNSS+ 2021)*, pages 725–752.

Jin, C., Bajaj, I., Zhao, K., Tay, W. P., and Ling, K. V. (2021). 5G Positioning Using Code-Phase Timing Recovery. In *2021 IEEE Wireless Communications and Networking Conference (WCNC)*, pages 1–7.

Mata, F., Grec, F., Azaola, M., Blázquez, F., Fernández, A., Dominguez, E., Cueto-Felgueroso, G., Seco-Granados, G., del Peral-Rosado, J., Staudinger, E., et al. (2020). Preliminary field trials and simulations results on performance of hybrid positioning based on GNSS and 5G signals. In *Proceedings of the 33rd International Technical Meeting of the Satellite Division of The Institute of Navigation (ION GNSS+ 2020)*, pages 387–401.

Orabi, M., Abdallah, A. A., Khalife, J., and Kassas, Z. M. (2021). A Machine Learning Multipath Mitigation Approach for Opportunistic Navigation with 5G Signals. In *Proceedings of the 34th International Technical Meeting of the Satellite Division of The Institute of Navigation (ION GNSS+ 2021)*, pages 2895–2909.

Renaudin, O., Salcedo, J. A. L., Seco-Granados, G., Lapin, I., Zanier, F., and Ries, L. (2021). TOA Error Bounds for Positioning in 5G New Radio Networks. In *Proceedings of the 34th International Technical Meeting of the Satellite Division of The Institute of Navigation (ION GNSS+ 2021)*, pages 2940–2956.

Shamaei, Kimia, Khalife, Joe, Kassas, and M, Z. (2016). Performance characterization of positioning in LTE systems. In *Proceedings of the 29th International Technical Meeting of the Satellite Division of The Institute of Navigation (ION GNSS+ 2016)*, pages 2262–2270.

Shamaei, K. and Kassas, Z. M. (2018). LTE receiver design and multipath analysis for navigation in urban environments. *Navigation*, 65(4):655–675.

Shamaei, K., Khalife, J., and Kassas, Z. M. (2018). Exploiting LTE signals for navigation: Theory to implementation. *IEEE Transactions on Wireless Communications*, 17(4):2173–2189.

Tobie, A.-M., Garcia-Pena, A., Thevenon, P., Vezinet, J., and Aubault, M. (2020). Hybrid navigation filters performances between GPS, Galileo and 5G TOA measurements in multipath environment. In *Proceedings of the 33rd International Technical Meeting of the Satellite Division of The Institute of Navigation (ION GNSS+ 2020)*, pages 2107–2140.

Yang, B., Letaief, K., Cheng, R., and Cao, Z. (2000). Timing recovery for OFDM transmission. *IEEE Journal on Selected Areas in Communications*, 18(11):2278–2291.

Yin, L., Ni, Q., and Deng, Z. (2018). A GNSS/5G Integrated Positioning Methodology in D2D Communication Networks. *IEEE Journal on Selected Areas in Communications*, 36(2):351–362.